

A $\log N_{\text{HI}} = 22.5$ DLA in a dark gamma-ray burst: the environment of GRB 050401¹

D. Watson,² J. P. U. Fynbo,² C. Ledoux,³ P. Vreeswijk,³ J. Hjorth,² K. Aoki,⁴
T. Augusteijn,⁵ A. P. Beardmore,⁶ D. Bersier,⁷ J. M. Castro Cerón,² P. D'Avanzo,^{8,9}
D. Diaz-Fraile,¹⁰ P. Hirst,¹¹ P. Jakobsson,² B. L. Jensen,² N. Kawai,¹² G. Kosugi,¹³
A. Levan,¹⁴ J. Masegosa,¹⁰ J. Näränen,⁵ K. L. Page,⁶ K. Pedersen,² A. Pozanenko,¹⁵
J. N. Reeves,^{16,17} V. Rumyantsev,¹⁸ T. Shahbaz,¹⁹ D. Sharapov,²⁰ A. Smette,^{3,21}
J. Sollerman,¹ R. L. C. Starling,²² N. Tanvir,¹⁵ K. Torstensson,⁵ and K. Wiersema²²

¹Based in part on observations made at the European Southern Observatory, Paranal, Chile under program 075.D-0270, with the Nordic Optical Telescope, operated on the island of La Palma jointly by Denmark, Finland, Iceland, Norway, and Sweden, in the Spanish Observatorio del Roque de los Muchachos of the Instituto de Astrofísica de Canarias, with the Wide Field Camera (WFCAM) on the United Kingdom Infrared Telescope, which is operated by the Joint Astronomy Centre on behalf of the U.K. Particle Physics and Astronomy Research Council, and on data collected at the Subaru Telescope, which is operated by the National Astronomical Observatory of Japan.

ABSTRACT

The optical afterglow spectrum of GRB 050401 (at $z = 2.8992 \pm 0.0004$) shows the presence of a large damped Ly α absorber (DLA), with $\log N_{\text{HI}} = 22.5 \pm 0.3$. This is the highest column density DLA ever observed, and is nearly an order

²Dark Cosmology Centre, Niels Bohr Institute, University of Copenhagen, Juliane Maries Vej 30, DK-2100 Copenhagen Ø, Denmark; darach@astro.ku.dk

³European Southern Observatory, Casilla 19001, Santiago 19, Chile

⁴Subaru Telescope, National Astronomical Observatory of Japan, 650 North A’ohoku Place, Hilo, HI 96720, USA

⁵Nordic Optical Telescope, Apartado 474, Santa Cruz de La Palma, Spain

⁶Department of Physics and Astronomy, University of Leicester, Leicester LE1 7RH, UK

⁷Astrophysics Research Institute, Liverpool John Moores University, Twelve Quays House, Egerton Wharf, Birkenhead, CH41 1LD, UK

⁸INAF, Osservatorio Astronomico di Brera, via E. Bianchi 46, I-23807 Merate (LC), Italy

⁹Dipartimento di Fisica e Matematica, Università dell’Insubria, via Valleggio 1 1, I-22100 Como, Italy

¹⁰Instituto de Astrofísica de Andalucía, CSIC, c/ Camino Bajo de Hueter 24, 18008 Granada, Spain

¹¹Joint Astronomy Centre, 660 North A’Ohoku Place, Hilo, HI 96720, USA

¹²Department of Physics, Tokyo Institute of Technology, 2-12-1 Ookayama, Meguro-ku, Tokyo 152-8551, Japan

¹³ALMA Project Office, National Astronomical Observatory of Japan, 2-21-1 Osawa, Mitaka, Tokyo, 181-8588, Japan

¹⁴Centre for Astrophysics Research, University of Hertfordshire, College Lane, Hatfield AL10 9AB, UK

¹⁵Space Research Institute (IKI) 117997, 84/32 Profsoyuznaya Str, Moscow, Russia

¹⁶Laboratory for High Energy Astrophysics, Code 662, NASA Goddard Space Flight Center, Greenbelt Road, Greenbelt, MD 20771, USA

¹⁷Universities Space Research Association

¹⁸Crimean Astrophysical Observatory, Ukraine

¹⁹Instituto Astrofísica de Canarias, c/ Via Lactea s/n, 38200 La Laguna, Tenerife, Spain

²⁰Ulugh Beg Astronomical Institute, Tashkent 700052, Uzbekistan

²¹Research Associate, FNRS, Belgium

²²Astronomical Institute ‘Anton Pannekoek’, University of Amsterdam, Kruislaan 403, 1098 SJ Amsterdam, the Netherlands

of magnitude larger than any DLA observed in QSO spectra. The early X-ray spectrum from *Swift*-XRT, shows a column density above the Galactic level equivalent to $\log N_{\text{H}} = 22.21_{-0.08}^{+0.06}$ with solar abundances and at $z = 2.8992$. The comparison of the X-ray column density measurement, which is dominated by metal absorption, and the optical H I column, allows us to derive a metallicity for the absorbing matter of $[X/H] = -0.3 \pm 0.3$. From the optical spectrum, we infer a zinc abundance of $[Zn/H] = -0.8 \pm 0.4$. We can then derive $[\alpha/Zn] = 0.5 \pm 0.2$, suggestive of an overabundance of α -elements in the absorber. There is evidence of dust depletion effects in the Fe, Si and Cr abundances and the optical spectrum is substantially reddened. This reddening can be well reproduced with an SMC extinction curve, with $A_V = 0.62 \pm 0.06$ (and cannot be reproduced with Galactic or LMC extinction). However the total extinction can also be constrained from the optical–X-ray spectral energy distribution, independent of assumptions about the shape of the extinction curve: $0.5 \lesssim A_V \lesssim 4.5$. This is less extinction than inferred from the soft X-ray absorption, $A_V = 9.1_{-1.5}^{+1.4}$. This discrepancy between the X-ray metal column density and the optical/UV absorption implies a low dust-to-metals ratio (specifically the α -chain elements). ‘Grey’ extinction cannot explain the discrepancy, even with an arbitrarily flat extinction curve (i.e. large absorption with little reddening). However, a large α -element overabundance can explain the discrepancy. If such overabundance is a feature common to afterglow absorbers it may explain the high X-ray column densities with little optical reddening observed in afterglow spectra, and would necessitate a cautious approach to interpreting dust properties based on metallicity arguments in these environments. A generally low dust-to-metals ratio surrounding GRBs may explain the dearth of heavily extinguished optical afterglows.

Subject headings: gamma rays: bursts—X-rays: general—galaxies: ISM—galaxies: high redshift—quasars: absorption lines—ISM: dust, extinction

1. Introduction

The largest H I column density absorption line systems [$N(\text{H I}) \geq 2 \times 10^{20} \text{ cm}^{-2}$], known as damped Ly α absorbers (DLAs), were first observed in QSO spectra, and originate in the H I regions of intervening galaxies (see Wolfe, Gawiser, & Prochaska 2005, for a recent review). Because background QSOs probe random sightlines through intervening galaxies, QSO-DLA systems can in principle be used as an unbiased tracer of the neutral gas at high redshift, gas that provides the fuel for star formation at these epochs (Lanzetta, Wolfe, &

Turnshek 1995; Wolfe et al. 1995) .

While QSO-DLAs have higher metallicities than other classes of intervening QSO absorbers (Pettini et al. 1994), typically, metallicities are low compared to solar metallicity, ($[X/H] \sim -1.5$ at $z \sim 3$) with a large scatter (Kulkarni & Fall 2002; Prochaska et al. 2003).

DLAs are also common in long duration γ -ray burst (GRB) afterglow spectra (Jensen et al. 2001; Hjorth et al. 2003a; Jakobsson et al. 2004b; Vreeswijk et al. 2004), typically with much higher column densities than observed in QSO-DLAs (Vreeswijk et al. 2004). It seems highly plausible, given that long-duration GRBs are known to have massive star progenitors (Stanek et al. 2003; Hjorth et al. 2003b), that the extremely large neutral hydrogen column densities observed in many GRB-DLAs are related to the GRBs’ star-forming regions (e.g. Bloom, Kulkarni, & Djorgovski 2002). This means that while the highest redshift absorption system in an afterglow spectrum belongs to the GRB host, and is unlikely to be useful as a random probe of intervening matter, it can instead provide rich information on the sites of active star-formation in the high-redshift universe (the mean and median redshifts of recent samples of GRBs are now very high, around $z = 2.8$, and the first GRB at $z > 6$ has recently been found; Jakobsson et al. 2005; Kawai et al. 2005; Tagliaferri et al. 2005; Price et al. 2005; Haislip et al. 2005; Watson et al. 2005). At the same time, afterglow spectra can still be used as random probes for intervening absorbers at lower redshifts in the same way as QSOs. The largest DLAs, as determined from $\text{Ly}\alpha$ measurements, in any DLA to date are found in GRB afterglows: GRB 030323 with $\log N_{\text{HI}} = 21.90 \pm 0.07$ (Vreeswijk et al. 2004) and more recently $\log N_{\text{HI}} = 22.1 \pm 0.1$ in the afterglow of GRB 050730 (Starling et al. 2005; Chen et al. 2005).

Further data on the birth matrix of GRBs are provided by studies of the afterglow’s optical extinction and soft X-ray absorption. The optical studies provide an opportunity to constrain the extinction law for star-forming galaxies at high redshift, though the work may be complicated by the possibility of destruction of dust grains by the GRB. Indeed it has been proposed that GRB afterglows are subject to a ‘flat’ or ‘grey’ extinction law due to a change in the grain size distribution caused by the sublimation and breaking of dust grains (Waxman & Draine 2000; Fruchter, Krolik, & Rhoads 2001; Perna, Lazzati, & Fiore 2003), i.e. where there is evidence for little spectral reddening but where the presence of a significant dust column is inferred. Proposed evidence for this includes large metal column densities observed in afterglows which exhibit little curvature in their optical afterglow spectra. The metal column densities are derived either from optical absorption lines (where dust depletion effects have also been observed, Savaglio, Fall, & Fiore 2003; Savaglio & Fall 2004), or from the soft X-ray absorption (Stratta et al. 2005, 2004), where the most important contribution comes from oxygen K-shell absorption. This apparent discrepancy between the metal column

density and the optical reddening was first observed in a careful and seminal paper by Galama & Wijers (2001), using very low quality X-ray spectra from *BeppoSAX*. The only alternatives to a flat extinction law appear to be a non-universal dust-to-metals ratio or possibly, in the case of the X-ray absorbers, a super-abundance of the α -chain elements.

To distinguish between these possibilities, we require a direct measure of both the soft X-ray and Ly α absorptions in a single GRB afterglow, observations that have been elusive because of the conflicting requirements of a relatively low redshift for an accurate determination of the intrinsic soft X-ray absorption, and high redshift to move Ly α to observable wavelengths.

In this paper we present X-ray and optical observations of GRB 050401 (§ 2), the resulting spectra and lightcurves (§ 3), and the implications of these observations (§ 4).

A cosmology with $\Omega_m = 0.3$, $\Omega_\Lambda = 0.7$ and $H_0 = 75 \text{ km s}^{-1} \text{ Mpc}^{-1}$ is assumed throughout. Error ranges quoted are 68% confidence intervals for one parameter of interest, unless otherwise indicated.

2. Observations and data reduction

On 1 April 2005 at 14:20:15 UT *Swift*'s Burst Alert Telescope (BAT) triggered on a multi-peaked burst with a duration of 33 ± 2 s (Barbier et al. 2005; Sakamoto et al. 2005). A rapid autonomous slew of the satellite resulted in the X-Ray Telescope (XRT) being on source within seconds and a bright, fading source was discovered in the BAT error-circle (Angelini et al. 2005). XRT revisited the source again on 6, 7 and 8 April. We acquired the XRT data from the archive and used the level 2 events files to construct the lightcurves and spectra, using a 40 pixel wide source extraction box for the Windowed Timing (WT) mode data with a background region box $4'$ away. A 12 pixel radius circle was used to extract the source counts in Photon Counting (PC) mode; an annulus around the source region was used to extract a background in this case. Data in PC mode with a source count rate above $0.4 \text{ counts s}^{-1}$ are likely to be affected by pile-up and were not used, as good statistics on the bright afterglow were available from the WT mode data. HEASOFT 6.0 was used to analyse and reduce the data with the latest calibration files. Ancillary response files were produced with `xrtmkarf` using ‘inarfile=CALDB’, but the fit to the data at energies close to 0.5 keV was poor. Running `xrtmkarf` with ‘inarfile=NONE’ produces an ancillary response file without using a modified on-axis ancillary response as input, instead using the mirror on-axis effective area and the filter transmission file directly. The ancillary response produced in this way improved the fit at low energies, though the results presented here are not strongly

Table 1: Optical and near-IR imaging observations

Date (UT)	Telescope	Mag	Time since trigger (ks)
R-band			
April 1.9880	MAO	22.7(2)	33.75
April 2.0720	TNG	23.0(1)	41.01
April 2.2100	VLT	23.27(9)	52.93
April 2.2243	NOT	23.0(2)	54.16
April 2.2563	VLT	23.31(8)	56.93
April 2.3004	VLT	23.44(8)	60.74
April 2.3183	D1.5	23.5(2)	62.29
April 2.3438	VLT	23.5(9)	64.49
April 3.2414	NOT	23.9(2)	142.0
April 8.2116	NOT	25.3(4)	571.5
April 14.5947	Subaru	26.0(1)	1123
J-band			
April 1.6402	UKIRT	18.6(2)	3.698
H-band			
April 1.6346	UKIRT	17.9(1)	3.214
April 1.6457	UKIRT	18.1(2)	4.173
April 1.6513	UKIRT	18.0(1)	4.657
April 2.3521	CTIO	20.3(1)	65.21
K-band			
April 1.6242	UKIRT	16.88(8)	2.316
April 1.6284	UKIRT	17.2(1)	2.678
April 14.2742	VLT	> 21.5	1095

Note. — Final digit uncertainties are listed in parentheses. Observations of the afterglow of GRB 050401 were obtained at the ESO Very Large Telescope (VLT), the 8.2 m Subaru telescope, the 2.5 m Nordic Optical Telescope (NOT), the Danish 1.54 m telescope (D1.5), Telescopio Nazionale Galileo (TNG), the 1.5 m telescope at the Maidanak Astronomical Observatory in Uzbekistan (MAO), the Blanco 4.0 m telescope at the Cerro Tololo Inter-American Observatory (CTIO), and the 3.8 m UK Infrared Telescope (UKIRT).

dependent on the choice of response file, in particular a very large excess column density is detected regardless of which ancillary response is used.

Optical and near-IR observations of the optical afterglow of GRB 050401 (McNaught & Price 2005) were secured at several telescopes (see Table 1). Starting at 5:16 UT on April 2, 2005 (14.9 hours after the burst trigger), 8 spectra of 1450 s each were acquired with the FORS2 instrument on Antu of the VLT, using the grism 300V and order sorting filter GG375, and a slit width of 1". This setting results in a pixel scale of 3.24 Å, and a FWHM resolution of 9.5 Å at 4000 Å and 11 Å at 9000 Å. After cosmic ray removal (see van Dokkum 2001), the spectra were reduced in the standard fashion, using IRAF. As the night was photometric, the GRB afterglow spectra were flux calibrated using the spectrophotometric standard star G138–31. Finally, the spectra were corrected for the Galactic foreground extinction estimate of $E(B-V) = 0.065$ mag of Schlegel, Finkbeiner, & Davis (1998). The resulting normalized spectrum and its 1σ error spectrum are shown in Fig. 1.

3. Results

3.1. The X-ray afterglow

The WT-mode data were fit with a power-law with fixed Galactic absorption ($4.8 \times 10^{20} \text{ cm}^{-2}$, using the `nh` ftool Dickey & Lockman 1990). The fit using this model was poor ($\chi^2/\text{dof} = 629/263$) leaving large negative residuals at low energies, and so an extra parameter, additional absorption at $z = 2.8992$ (the redshift of the burst—see below), was added to the fit. This improved the fit significantly ($\chi^2/\text{dof} = 297/262$), and gave best-fit values of photon spectral index $\Gamma = 1.89 \pm 0.03$ and equivalent hydrogen column density $N_{\text{H}} = 1.6 \pm 0.1 \times 10^{22} \text{ cm}^{-2}$ ($\log N_{\text{H}} = 22.20 \pm 0.03$). Using the ancillary response file created with ‘`xrtmkarf inarffile=CALDB`’, the best-fit values were consistent— $\Gamma = 1.85 \pm 0.03$ and $N_{\text{H}} = 1.6 \pm 0.2 \times 10^{22} \text{ cm}^{-2}$. The absorbing column density is fit using the absorption cross-sections of Morrison & McCammon (1983), which assumes solar abundances. Splitting the WT-mode data in three equally long-lasting bins revealed no significant change in the spectrum (absorbing column or spectral slope).

The level of the Galactic foreground absorption may be uncertain up to $\sim 20\%$ (Dickey & Lockman 1990). Including this uncertainty leads to a more conservative error estimate of $N_{\text{H}} = 1.6 \pm 0.3 \times 10^{22} \text{ cm}^{-2}$ for the equivalent hydrogen column density.

Although the X-ray column density is usually expressed in terms of the equivalent hydrogen column density, this assumes solar metallicities; the soft X-ray absorption is in fact a direct measure of the total metal column density in the solid and gas phases. The

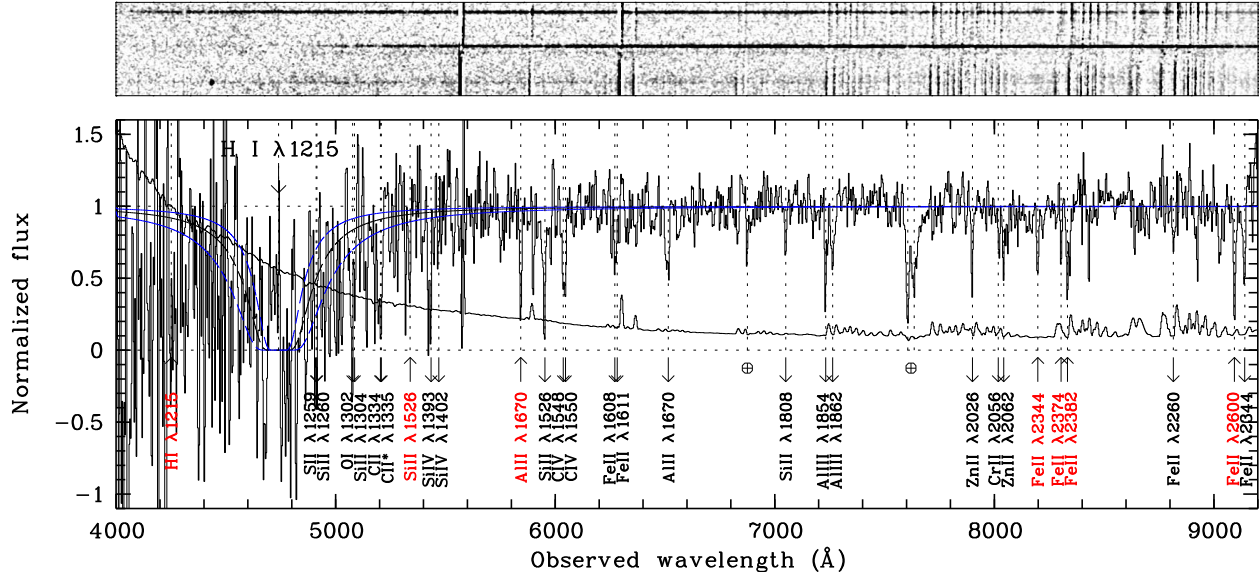


Fig. 1.— *Lower panel:* VLT/FORS2 spectrum of GRB 050401 obtained 15 hours after the burst when the afterglow was at a magnitude of $R = 23.2$. There are two absorption systems at $z = 2.9$ (black labels, down arrows) and $z = 2.5$ (grey labels, up arrows). The DLA at $z = 2.9$ is the largest ever observed and has a metallicity approximately $1/10^{\text{th}}$ of the solar value ($[Zn/H] = -0.8 \pm 0.4$). The fit to the spectrum corresponds to a column density of $\log N_{\text{HI}} = 22.5 \pm 0.3$. The 1σ error spectrum is also shown. *Upper panel:* The 2 dimensional spectrum covering the same wavelength range as the 1 dimensional spectrum in the lower panel. The spectrum in the middle is the afterglow. Above and below are the spectra of 2 other objects on the slit. The spectrum of the object above the afterglow spectrum extends far bluewards of where the afterglow spectrum falls off. The spectrum below the afterglow spectrum is most likely due to a $z = 2.65$ Ly α emitter.

biggest contribution to the absorption comes from the oxygen K-shell absorption edges, with O I at 0.52 keV. There is also a significant contribution from other α -chain elements. For instance, at $z \sim 3$ the oxygen and other α -elements are responsible for two-thirds of the absorption in a typical X-ray CCD spectrum (e.g. *Swift*-XRT) at solar abundances. The X-ray column density is therefore effectively a measure of the α -element column (see also Morrison & McCammon 1983; Galama & Wijers 2001; Turnshek et al. 2003). It is very often impossible to determine the ionisation state of the X-ray absorber due to Galactic absorption, the fact that at moderate redshifts the oxygen edge is usually shifted out of the bandpass of most X-ray detectors, and the low resolution of CCD X-ray spectra. This, combined with the fact that the difference in the measured absorbing column density is expected to be small for neutral or low ionisation states means that column density measures from soft X-rays are given for a neutral column. The fact that we do not know the ionisation state of the X-ray absorber can lead to uncertainties in the metal abundance determinations. However as there is evidence of a large, neutral column density and no evidence for a significant highly ionised column, this is likely to be a negligible source of error (see also Turnshek et al. 2003).

The 0.2–10.0 keV lightcurve (Fig. 2) is not well fit by a single power-law ($\chi^2/\text{dof} = 721.3/65$) but a broken power-law improves the fit significantly ($\chi^2/\text{dof} = 93.4/63$) with a break at 4400 ± 400 s, from a decay index $\alpha_{X1} = 0.65 \pm 0.02$ to $\alpha_{X2} = 1.39_{-0.04}^{+0.05}$. There is no significant change in the spectrum from one side of the break to the other, although the spectrum on the late side of the break has low number counts and is not as well-constrained as the early spectrum.

3.2. Optical Photometry and Spectroscopy

The optical lightcurve (Fig. 2) is well fit with a single power-law ($\chi^2/\text{dof} = 11.5/11$) with decay index $\alpha_O = 0.82 \pm 0.03$. This fit is consistent with data from less than a minute (the burst was observed very rapidly by ROTSE-IIIa, Rykoff et al. 2005) to nearly two weeks post-burst. Such a uniform decay is unusual for optical afterglows that typically display one or more breaks in this time interval. Furthermore, this optical decay slope is significantly different from both X-ray decay slopes. The uniformity of the decay, however, and the similarity with the H-band decay ($\alpha_H = 0.76 \pm 0.04$) means that we can have considerable confidence in the correction of the optical/NIR data to an epoch common to the X-ray observations in order to construct the spectral energy distribution (SED).

A striking feature in the Galactic-extinction-corrected, flux-calibrated optical spectrum is that it is very red compared to typical optical afterglow spectra (Fig. 3). The best-fit spectral index ($F_\nu \propto \nu^{-\beta}$) is $\beta_O = 2.8$ (fitting only the spectral range 5800–9000Å). This

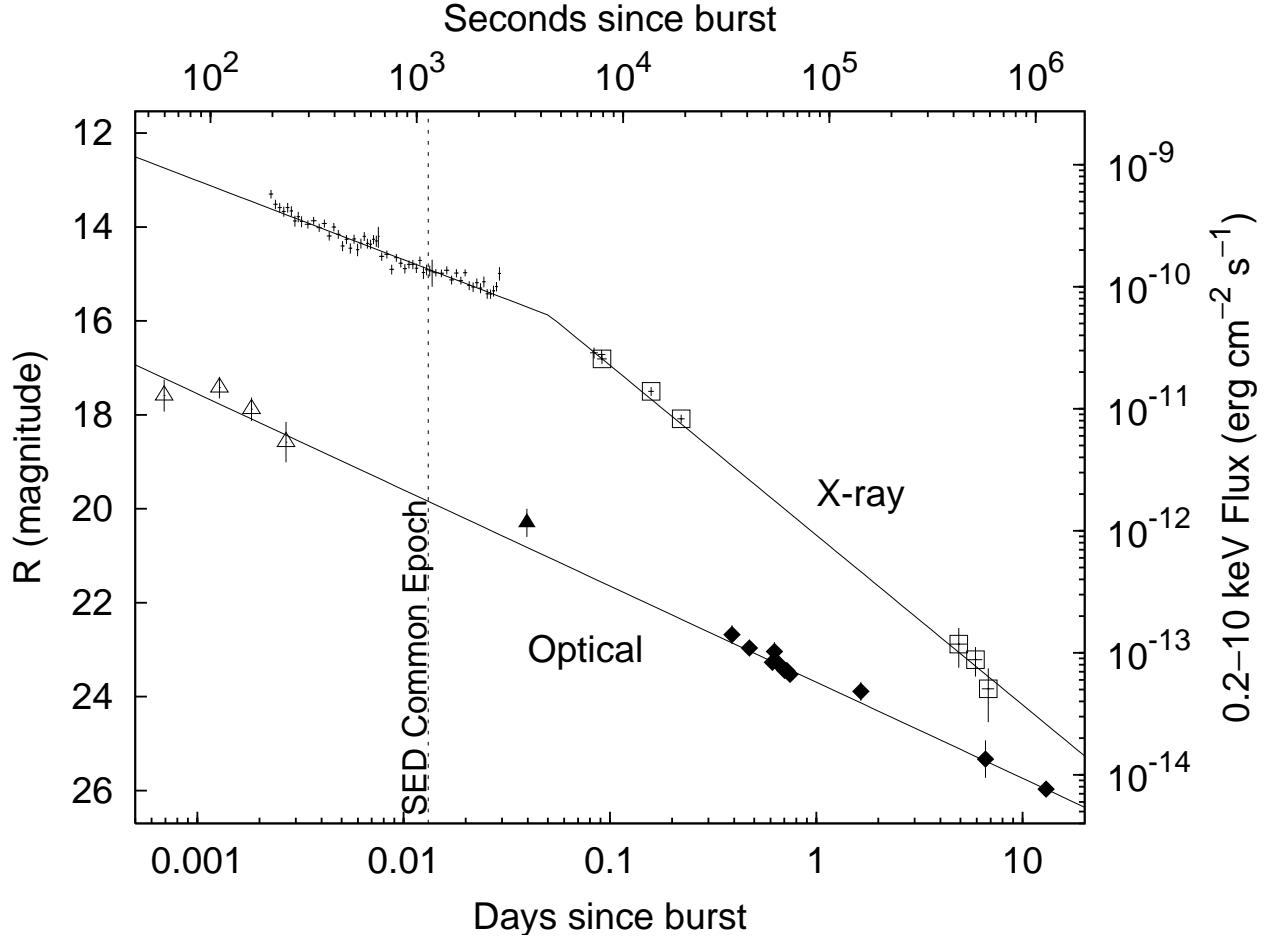


Fig. 2.— X-ray and optical lightcurves of the afterglow of GRB 050401. The R-band lightcurve (left axis, diamonds) is well fit by a single power-law with index $\alpha_O = 0.82$. This fit is consistent with data beginning at less than one minute after the burst, from Rykoff et al. (2005, open triangle) and McNaught & Price (2005, filled triangle) though they are not included in the fit. The observed X-ray lightcurve (right axis, WT mode—crosses, PC mode—boxes) requires a break at 4400 s with α_X changing from 0.65 to 1.39. The epoch to which the data were interpolated to produce the SED is indicated with a dashed line.

fact, coupled with an optical-to-X-ray spectral index (β_{OX}) of 0.2, strongly suggests that the optical spectrum is reddened by dust. SMC, LMC and Galactic extinction laws (Pei 1992) were fit to the optical spectrum assuming an underlying power-law continuum. As with all GRB afterglows studied to date, lack of a 2174 Å bump in the spectrum means that SMC extinction fits the continuum spectrum best (e.g. Vreeswijk et al. 2004; Jakobsson et al. 2003; Savaglio & Fall 2004), yielding an intrinsic power-law spectral index, $\beta_{\text{O}} = 0.5 \pm 0.2$ and $A_V = 0.62 \pm 0.06$.

The other striking feature in the spectrum is the large absorption edge beginning near 5400 Å. Given the metal absorption line systems detected in the spectrum (Fig. 1), with redshifts of $z = 2.5$ and $z = 2.9$, we interpret this as the red wing of very high column density H I Ly α absorption at $z_{\text{abs}} = 2.89$. Fitting a damped Ly α profile to the red wing yields a column density of $\log N_{\text{HI}} = 22.5 \pm 0.3$. This is the largest DLA ever observed, larger even than observed in GRB 050730 (Starling et al. 2005; Chen et al. 2005) and GRB 030323 (Vreeswijk et al. 2004) and an order of magnitude larger than observed in any QSO-DLA (Curran et al. 2002). Among the metal absorption lines observed in the optical spectrum, the Zn II doublet at $z_{\text{abs}} = 2.8992$ is unambiguously identified. The observed equivalent width of the Zn II $\lambda 2026$ line is 6 ± 1 Å. Since this line may be saturated, the corresponding Zn metallicity, $[\text{Zn}/\text{H}] = -1.24$, derived from the optically thin limit approximation, should be considered as a lower limit. We tentatively performed simultaneous Voigt profile fitting of these lines together with carefully selected, weak and unblended lines from Cr II, Si II and Fe II (Fig. 4). A best-fit redshift of 2.8992 ± 0.0003 is found as well as an effective Doppler parameter $b = 62 \pm 21 \text{ km s}^{-1}$. Best-fitting column densities are given in Table 2. From this fit we find $[\text{Zn}/\text{H}] = -0.8 \pm 0.4$, taking into account the 0.3 dex uncertainty on the determination of N_{HI} . This metallicity is similar to or higher than the few previous measurements for other GRBs at similar redshifts (e.g. Savaglio et al. 2003; Vreeswijk et al. 2004; Prochaska et al. 2004; Starling et al. 2005; Chen et al. 2005) and is different from the metallicity obtained from the X-ray column density: $(\log N_{\text{H}} = 22.21_{-0.08}^{+0.06})$ for a solar metallicity. This implies a metallicity lower than solar: $[\text{X}/\text{H}] = -0.3 \pm 0.3$, and is discussed below in § 4.

We note that there is an intervening absorption system at $z = 2.50$ based on Si II, Al II, and Fe II lines. In the 2 dimensional spectrum we also identify a Ly α emitter at $z = 2.65$ at an impact parameter of 10.2" south of the GRB position (81.3 kpc at $z = 2.65$, see the upper panel in Fig. 1). There is no significant absorption in the afterglow spectrum at this redshift. There is also no evidence for Ly α emission from the host galaxy in the 2D spectrum, but as the host galaxy is not detected this does not exclude even a large equivalent width Ly α emission line from the host.

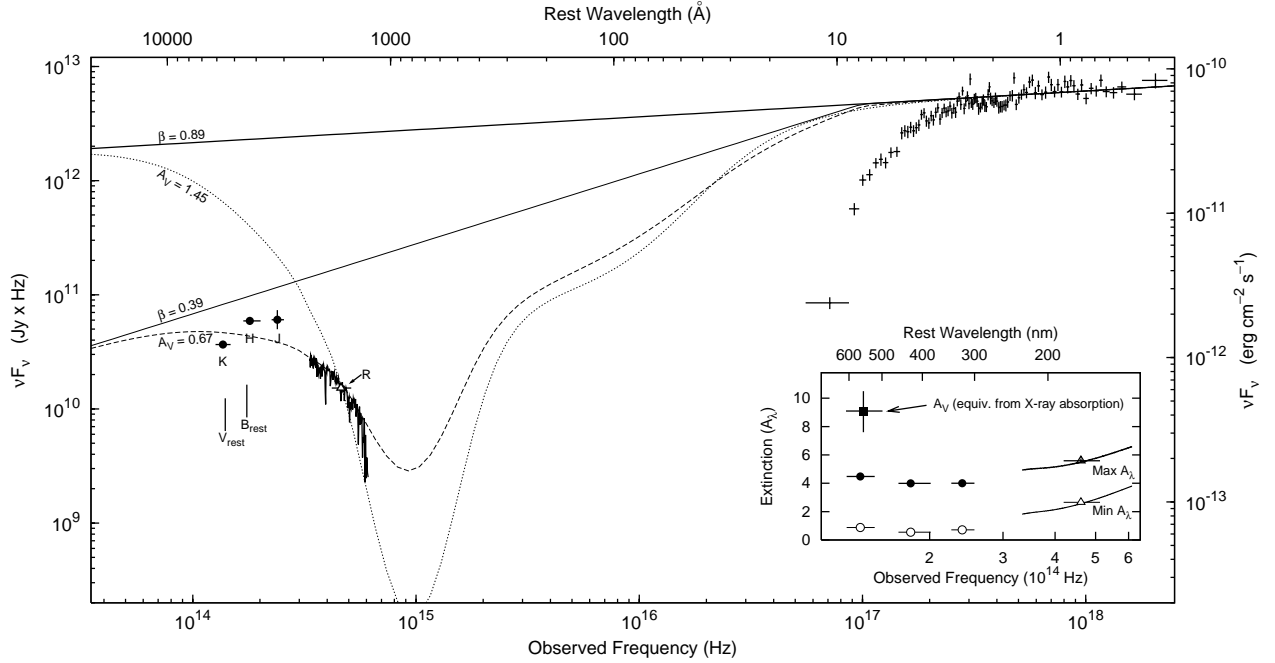


Fig. 3.— The spectral energy distribution of the afterglow of GRB 050401. The best-fit power-law to the X-ray data is plotted over the X-ray data and extrapolated across the frequency range of the optical spectrum and the near-IR and optical photometry, all of which have been interpolated to a common epoch of 18.9 minutes after the burst using the R-band lightcurve. A broken power-law with the break set conservatively (minimising the required absorption) at 0.4 keV is also plotted. The extinction (SMC curve, $A_V = 0.67$) of the broken power-law that best reproduces the optical spectrum, assuming a power-law with $\beta = 0.39$ (rebinned by a factor of ten here) is plotted as a dashed line. The SMC extinction required to account for the R-band data assuming the single power-law continuum extrapolated from the X-rays ($A_V = 1.45$) is plotted as a dotted line for comparison. *Inset.* The maximum and minimum extinctions as a function of wavelength (single and broken power-laws divided by the observed data). Circles represent the observed NIR data, triangles the observed R-band, and the solid curve the continuum from the spectral observations. The extinction expected from the soft X-ray absorption measurement is plotted as a filled square. The inconsistency of the optical/NIR limits with the extinction expected from the X-ray absorption appears to suggest either an overabundance of α -elements or a non-universal dust-to-metals ratio.

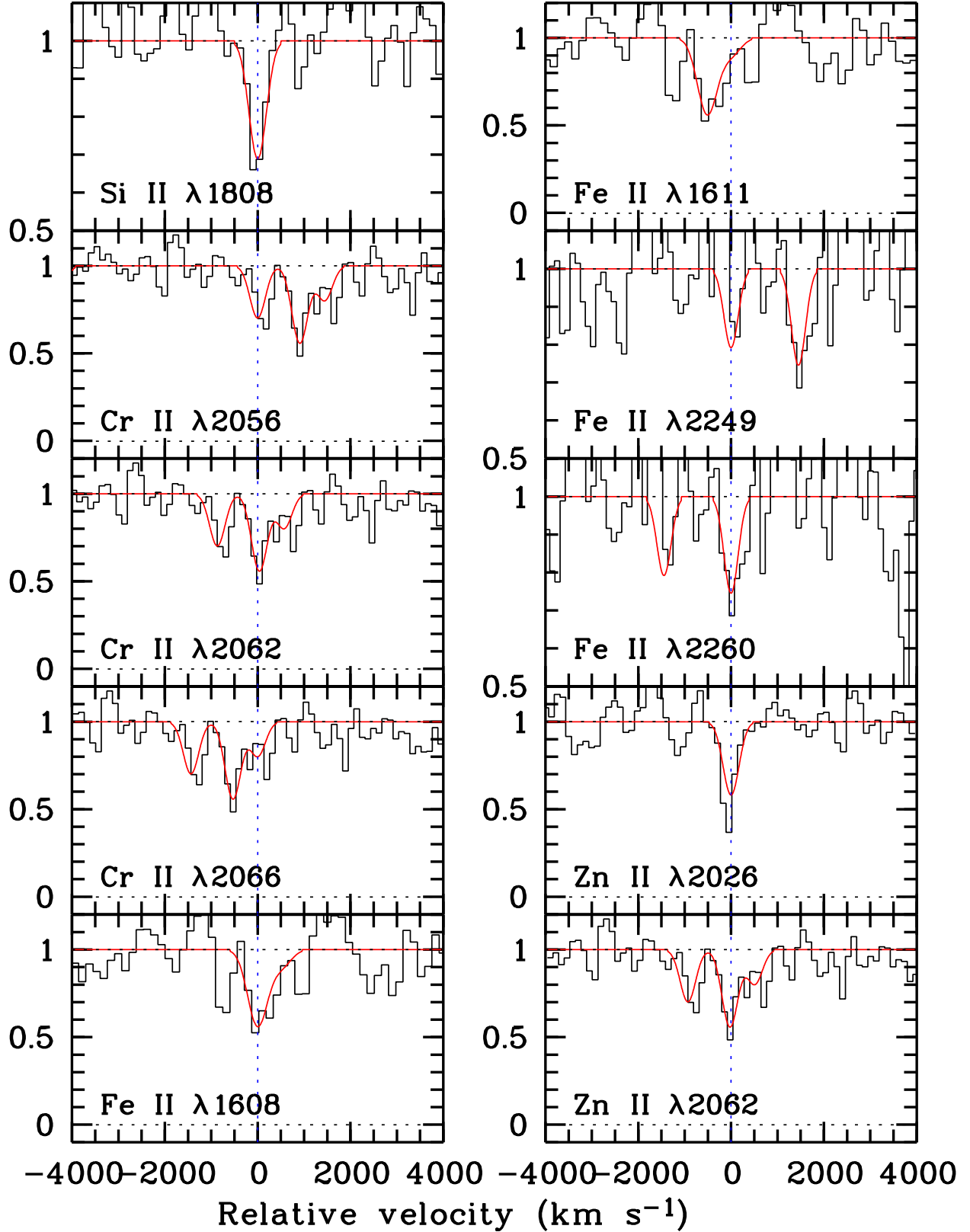


Fig. 4.— Simultaneous Voigt-profile fitting of carefully selected, weak and unblended absorption lines observed at $z_{\text{abs}} = 2.8992$ in the afterglow spectrum of GRB 050401. The zero of the velocity scale corresponds to this redshift.

3.3. The spectral energy distribution

The photon-weighted mean time of the WT-mode X-ray spectrum was 1136 s after the burst. The flux of the optical spectrum was interpolated to this time, using the $\alpha_O = 0.82$ decay slope and the flux calibration of the spectrum. The best-fit to the R-band lightcurve is consistent with the flux interpolation of the optical spectrum to this time (Fig. 3). The NIR data were also corrected to this time, assuming their decay was the same as the R-band decay rate. The correction in the NIR was less than for the optical spectrum since the NIR observations occurred between 37 and 76 minutes after the burst.

The SED (Fig. 3) clearly shows that a break in the optical–X-ray spectral index is required even to fit a simple SMC extinction-correction to the optical spectrum alone. Larger absorption with less reddening would of course allow the optical spectrum to be fit if we assume an intrinsic optical slope that was a continuation of the the X-ray slope. Such an extinction would be consistent with the idea of a flat or ‘grey’ extinction as advocated by Galama & Wijers (2001), Savaglio & Fall (2004) and Stratta et al. (2005) among others. The limits on the extinction for GRB 050401 were derived from the extreme cases of 1) a single power-law extrapolated from the X-ray spectrum to the optical ($\beta = 0.89$) and 2) a broken power-law with a $\Delta\beta = -0.5$ (giving $\beta = 0.39$), as expected from the fireball model (Sari, Piran, & Narayan 1998), with the break set conservatively just inside the observed X-ray band (0.4 keV). These limits are shown in the inset to Fig 3. It is notable that a flat extinction curve alone cannot reconcile the maximum extinction inferred from the SED with the large metal absorbing columns we observe, if we maintain a universal dust-to-metals ratio. We discuss this conflict below.

4. Discussion

The optical afterglow of GRB 050401 is particularly faint—in fact it is the faintest GRB afterglow for which an absorption line redshift has been obtained. The observed optical to X-ray spectral slope is flatter than expected for the fireball model, therefore GRB 050401 falls into the ‘dark burst’ population as defined by Jakobsson et al. (2004a). The observed reddening in the optical spectrum and the discrepant X-ray-optical SED allow us to conclude that the ‘dark’ nature of the burst can be explained by extinction in the host galaxy. It is interesting that the very high column densities observed in GRB hosts, which are probably local to the GRBs, means that we do not need to invoke very dusty environments to explain dark bursts—these very high column densities containing only a modest amount of dust would be enough to darken the afterglow below the detectability threshold in many cases.

Since we expect GRB progenitors to be short-lived (Woosley & Heger 2005), the cloud probed by the afterglow is likely to be the matrix out of which the progenitor was born. For this reason, it would be problematic to try to infer the global properties of the ISM at high-redshift from the GRB’s probable host DLA as is done with QSO-DLAs. But for exactly the same reason GRB-DLAs are particularly important for determining the nature of the progenitor material of the GRB. For instance, the favoured model of long duration GRBs (the ‘collapsar’, Woosley 1993; Woosley & Heger 2005), predicts that GRBs should generally be found in low metallicity environments.

Previous observations of GRB afterglows have suggested that GRBs reside in low metallicity galaxies (Fynbo et al. 2003; Prochaska et al. 2004), and in fact the two next largest GRB-DLAs after GRB 050401 have a metallicity roughly $[X/H] = -2$ (Vreeswijk et al. 2004; Starling et al. 2005; Chen et al. 2005). The absorbers in GRB afterglows usually have high metal column densities, but relatively little reddening—this phenomenon is often attributed to a flat extinction law, probably due to destruction of dust grains (Galama & Wijers 2001; Fruchter et al. 2001; Savaglio & Fall 2004; Stratta et al. 2005).

Here we have one of the first direct measures in a single GRB of the H I column density and the total metal (primarily α -element) column density. This allows us to constrain the metallicity from the X-ray measurement, suggesting $[X/H] = -0.3 \pm 0.3$, where most of the uncertainty is in the hydrogen column. Using the best-fit to the optical absorption lines we find $[Zn/H] = -0.8 \pm 0.4$. Zn is one of the elements least affected by depletion onto dust grains and should be a good tracer of the Fe-group metallicity. By fixing the column density at the level of the optically-determined H I column density and the Fe-group elements at the level determined from the Zn abundance, we can fit for the α -element abundance in the X-ray spectrum. We obtain $\alpha = 0.44 \pm 0.05 Z_{\odot}$, which translates to $[\alpha/H] = 0.4 \pm 0.3$, including the H I uncertainty. We can also obtain a direct X-ray to optical metallicity measurement ratio, without going through the comparison with the hydrogen column (which introduces considerable extra uncertainty). This ratio implies an overabundance of α -elements to Zn compared to solar: $[\alpha/Zn] = 0.5 \pm 0.2$, or a factor of 3 ± 1 .

In an analysis of AGN absorbers, Turnshek et al. (2003) invoke an overabundance of α -chain to Fe-group elements of 2.5. Such an overabundance could explain the results observed here. Indeed, this degree of α -element overabundance seems expected in a DLA with the relatively high Zn metallicity observed here (see Turnshek et al. 2003), and indicates a relatively young ISM still dominated by products from core collapse rather than type Ia supernovae. The high α -element abundance can therefore be viewed as circumstantial supporting evidence for a Fe-group metallicity roughly $0.1 Z_{\odot}$ in the ISM of the GRB host.

From the optical measurements, there is no clear evidence for an overabundance of Si

compared to Zn, with $[\text{Si}/\text{Zn}] = -0.7 \pm 0.4$, but since Si can be depleted onto dust grains, this ratio probably reflects differential dust depletion effects. Evidence for a relatively strong dust depletion comes from iron for which we measure $[\text{Fe}/\text{Zn}] = -1.2 \pm 0.3$.

A possibility different from an overabundance of α -chain elements in the general ISM, is that the matter that dominates the absorption is very close to the progenitor and could perhaps be the cast-off, α -enriched envelope of the star itself. While it is expected that such material could have a moderate outflow velocity, a blueshift might not be noticeable without detecting the general ISM of the host galaxy itself. The suggestion is given a little added weight by the high densities in the very large DLA in GRB 050730 (Chen et al. 2005). If progenitor material is responsible for the X-ray absorption in some long GRBs, it is interesting to speculate on an open problem in GRB science: that soft X-ray emission lines may be related to this matter (Reeves et al. 2002; Watson et al. 2003; Butler et al. 2003).

In spite of the relatively high metallicity (in Zn as well as α -elements) and the exceptionally high column density, the optical extinction is well fit using an SMC extinction curve with only $A_V = 0.62 \pm 0.06$ with an intrinsic slope, $\beta = 0.5 \pm 0.2$ (with a slightly flatter slope of $\beta = 0.39$ the required extinction is slightly higher, $A_V = 0.67$, Fig. 3). This is less than might be expected (at $\sim 95\%$ confidence) from a simple translation of the optical H I column to extinction, which would suggest $A_V = 2.3^{+1.9}_{-1.2}$ assuming an SMC dust-to-gas ratio (Bouchet et al. 1985). In a less model-dependent way, a direct comparison can be made between the optical spectrum and the optical-to-X-ray SED, thereby placing bounds on the total and selective extinctions (see Fig. 3 inset). $A_V < 0.5$ is excluded: it would require a non-power-law continuum in the optical which was also substantially below the continuum expected from the X-ray spectrum, even with a steep spectral break. On the other hand, $A_V > 4.5$ requires not only an extremely flat extinction curve, but also that the optical and X-ray afterglows are driven by different emission components. These limits ($4.5 > A_V > 0.5$) are at odds with the A_V inferred from the soft X-ray absorption, which is $9.1^{+1.4}_{-1.5}$ (Predehl & Schmitt 1995). Since the X-ray absorption is dominated by metals, this conversion is not sensitive to a hydrogen-to-metals conversion. Allowing an α -element overabundance as suggested above could make the X-ray absorption and the extinction limits compatible, but this requires a very flat extinction curve unless the overabundance is large (a factor of ~ 10). We note that such overabundance has been suggested based on modelling of GRB progenitors (Yoon & Langer 2005). Alternatively, we may have a dust-to-metals ratio in the DLA an order of magnitude smaller than observed in the Galaxy or Magellanic clouds. But such a small dust-to-metals ratio is rather extreme given the relatively high metallicity in the DLA and the suggestion of dust depletion in the Si and Cr abundances. Of course, if the absorbing matter was mostly contributed by the progenitor, it seems natural that the matter could be dust-poor.

5. Conclusions

We have reported the largest DLA observed to date, in the GRB 050401. The metallicity is on the high side for a GRB-DLA, with $[\text{Zn}/\text{H}] = -0.8 \pm 0.4$. Large X-ray absorption is also detected, from which we infer a probable overabundance of α -chain elements of about 2.5 relative to the Zn abundance in the host galaxy ISM. Such an overabundance can be expected with this level of the Zn metallicity in DLAs. The extinction required by the X-ray absorbing column density exceeds the total extinction allowed by the SED in GRB 050401, and is more than an order of magnitude greater than the extinction inferred from a good fit of the SMC extinction curve to the reddening in the optical spectrum. A grey or flat extinction law is not sufficient to explain this discrepancy. We can conclude two things from this. 1) That even where SMC-type reddening fits an optical afterglow spectrum well, this does not necessarily imply that it is a reliable indicator of the total extinction. 2) Grey or flat extinction cannot be inferred from a high X-ray absorbing column coupled with little apparent reddening in the optical/UV. Dust destruction can also therefore not be inferred from this; it may simply imply an overabundance of oxygen and other α -chain elements. The dust-to-metals ratios observed in Galactic/Magellanic Cloud environments do not appear universal in GRB afterglow absorbers (see also Vladilo 2004); inferences on dust properties based on comparisons of optical reddening and metallicity therefore need to be approached cautiously.

We thank Peter Capak for excellent support of our CTIO observations. The Dark Cosmology Centre is funded by the DNERF. We acknowledge benefits from collaboration within the EU FP5 Research Training Network, ‘Gamma-Ray Bursts: An Enigma and a Tool’.

REFERENCES

- Angelini, L., et al. 2005, GCN Circ., 3161
- Barbier, L., et al. 2005, GCN Circ., 3162
- Bloom, J. S., Kulkarni, S. R., & Djorgovski, S. G. 2002, AJ, 123, 1111
- Bouchet, P., Lequeux, J., Maurice, E., Prevot, L., & Prevot-Burnichon, M. L. 1985, A&A, 149, 330
- Butler, N. R., Marshall, H. L., Ricker, G. R., Vanderspek, R. K., Ford, P. G., Crew, G. B., Lamb, D. Q., & Jernigan, J. G. 2003, ApJ, 597, 1010

- Chen, H.-W., Prochaska, J. X., Bloom, J. S., & Thompson, I. B. 2005, *ApJL* in press, astro-ph/0508270
- Curran, S. J., Webb, J. K., Murphy, M. T., Bandiera, R., Corbelli, E., & Flambaum, V. V. 2002, *Publications of the Astronomical Society of Australia*, 19, 455
- Dickey, J. M. & Lockman, F. J. 1990, *ARA&A*, 28, 215
- Fruchter, A., Krolik, J. H., & Rhoads, J. E. 2001, *ApJ*, 563, 597
- Fynbo, J. P. U., et al. 2003, *A&A*, 406, L63
- Galama, T. J. & Wijers, R. A. M. J. 2001, *ApJ*, 549, L209
- Haislip, J., et al. 2005, astro-ph/0509660
- Hjorth, J., et al. 2003a, *ApJ*, 597, 699
- Hjorth, J., et al. 2003b, *Nat*, 423, 847
- Jakobsson, P., et al. 2003, *A&A*, 408, 941
- Jakobsson, P., Hjorth, J., Fynbo, J. P. U., Watson, D., Pedersen, K., Björnsson, G., & Gorosabel, J. 2004a, *ApJ*, 617, L21
- Jakobsson, P., et al. 2004b, *A&A*, 427, 785
- Jakobsson, P., et al. 2005, astro-ph/0509888
- Jensen, B. L., et al. 2001, *A&A*, 370, 909
- Kawai, N., Yamada, T., Kosugi, G., Hattori, T., & Aoki, K. 2005, *GCN Circ.*, 3937
- Kulkarni, V. P. & Fall, S. M. 2002, *ApJ*, 580, 732
- Lanzetta, K. M., Wolfe, A. M., & Turnshek, D. A. 1995, *ApJ*, 440, 435
- McNaught, R. & Price, P. A. 2005, *GCN Circ.*, 3163
- Morrison, R. & McCammon, D. 1983, *ApJ*, 270, 119
- Pei, Y. C. 1992, *ApJ*, 395, 130
- Perna, R., Lazzati, D., & Fiore, F. 2003, *ApJ*, 585, 775
- Pettini, M., Smith, L. J., Hunstead, R. W., & King, D. L. 1994, *ApJ*, 426, 79

- Predehl, P. & Schmitt, J. H. M. M. 1995, *A&A*, 293, 889
- Price, P. A., Cowie, L. L., Minezaki, T., Schmidt, B. P., Songaila, A., & Yoshii, Y. 2005, [astro-ph/0509697](#)
- Prochaska, J. X., et al. 2004, *ApJ*, 611, 200
- Prochaska, J. X., Gawiser, E., Wolfe, A. M., Castro, S., & Djorgovski, S. G. 2003, *ApJ*, 595, L9
- Reeves, J. N., et al. 2002, *Nat*, 416, 512
- Rykoff, E. S., et al. 2005, *ApJ*, 631, L121
- Sakamoto, T., et al. 2005, *GCN Circ.*, 3173
- Sari, R., Piran, T., & Narayan, R. 1998, *ApJ*, 497, L17
- Savaglio, S. & Fall, S. M. 2004, *ApJ*, 614, 293
- Savaglio, S., Fall, S. M., & Fiore, F. 2003, *ApJ*, 585, 638
- Schlegel, D. J., Finkbeiner, D. P., & Davis, M. 1998, *ApJ*, 500, 525
- Stanek, K. Z., et al. 2003, *ApJ*, 591, L17
- Starling, R. L. C., et al. 2005, *A&A*, 442, L21
- Stratta, G., Fiore, F., Antonelli, L. A., Piro, L., & De Pasquale, M. 2004, *ApJ*, 608, 846
- Stratta, G., Perna, R., Lazzati, D., Fiore, F., Antonelli, L. A., & Conciatore, M. L. 2005, [astro-ph/0506411](#)
- Tagliaferri, G., et al. 2005, [astro-ph/0509766](#)
- Turnshek, D. A., Rao, S. M., Ptak, A. F., Griffiths, R. E., & Monier, E. M. 2003, *ApJ*, 590, 730
- van Dokkum, P. G. 2001, *PASP*, 113, 1420
- Vladilo, G. 2004, *A&A*, 421, 479
- Vreeswijk, P. M., et al. 2004, *A&A*, 419, 927
- Watson, D., et al. 2005, [astro-ph/0509640](#)

Watson, D., Reeves, J. N., Hjorth, J., Jakobsson, P., & Pedersen, K. 2003, *ApJ*, 595, L29

Waxman, E. & Draine, B. T. 2000, *ApJ*, 537, 796

Wolfe, A. M., Gawiser, E., & Prochaska, J. X. 2005, *ARA&A*, 43, 861

Wolfe, A. M., Lanzetta, K. M., Foltz, C. B., & Chaffee, F. H. 1995, *ApJ*, 454, 698

Woosley, S. & Heger, A. 2005, *astro-ph/0508175*

Woosley, S. E. 1993, *ApJ*, 405, 273

Yoon, S.-C. & Langer, N. 2005, *astro-ph/0508242*

Table 2: Absorption line fits at $z = 2.8992$

Central (Å) Wavelength	$\log N$ (cm^{-2})	ID	[X/H]	[X/Zn]
7049.8(5)	16.5(4)	Si II 1808	-1.5(5)	-0.7(4)
7900.3(6)	14.4(2)	Zn II 2026	-0.8(4)	
8042.7(6)	14.4(2)	Zn II 2062		
6271.7(5)	16.0(2)	Fe II 1608	-2.0(4)	-1.2(3)
6282.4(5)	16.0(2)	Fe II 1611		
8772.7(6)	16.0(2)	Fe II 2249		
8815.2(7)	16.0(2)	Fe II 2260		
8017.8(6)	14.6(2)	Cr II 2056	-1.6(4)	-0.8(3)
8041.1(6)	14.6(2)	Cr II 2062		
8056.4(6)	14.6(2)	Cr II 2066		

Note. — The uncertainty in the last digit is listed in parentheses.